Bio-Inspired Adaptive Sensing through Electropolymerization of Organic Electrochemical Transistors

Mahdi Ghazal, Michel Daher Mansour, Corentin Scholaert, Thomas Dargent, Yannick Coffinier, Sébastien Pecqueur, F. Alibart

ADVANCED ELECTRONIC MATERIALS
www.advelectronicmat.de

Bio-Inspired Adaptive Sensing through Electropolymerization of Organic Electrochemical Transistors

Mahdi Ghazal, Michel Daher Mansour, Corentin Scholaert, Thomas Dargent, Yannick Coffinier, Sébastien Pecqueur, and Fabien Alibart**

Organic electrochemical transistors are considered today as a key technology to interact with a biological medium through their intrinsic ionic-electronic coupling. In this paper, the authors show how this coupling can be finely tuned (in operando) post-microfabrication via the electropolymerization technique. This strategy exploits the concept of adaptive sensing where both transconductance and impedance are tunable and can be modified on-demand to match different sensing requirements. Material investigation through Raman spectroscopy, atomic force microscopy, and scanning electron microscopy reveals that electropolymerization can lead to a fine control of poly(3,4-ethylenedioxythiophene) (PEDOT) microdomains organization, which directly affects the iono-electronic properties of organic electrochemical transistors (OECTs). They further highlight how volumetric capacitance and effective mobility of PEDOT:polystyrene sulfonate influence distinctively the transconductance and impedance of OECTs. This approach shows to improve the transconductance by 150% while reducing their variability by 60% in comparison with standard spin-coated OECTs. Finally, they show how the technique can influence voltage spike rate hardware classification with direct interest in bio-signals sorting applications.

1. Introduction

Organic electro-chemical transistors (OECTs) have emerged as a key technology in both bio-sensing and neuromorphic engineering.[1–3] As bio-sensors, OECTs offer very attractive solutions for converting ionic signals into electronic ones thanks to the unique property of organic mixed ionic-electronic conductors (OMIECs).[4] Ionic concentration from an analyte or ionic currents from electroactive cells can be efficiently sensed/probed and amplified, thus making OECTs attractive sensors.[5] In the perspective of neuromorphic engineering, the same devices are capitalizing on the possibility to engineer devices where ion–electron coupling can be used to implement various synaptic plasticities, from short-term to long-term memory effects.[3,6–9] These two aspects have been so far mostly developed independently from each other. In contrast, synapses in biology are combining sensing capabilities with plastic properties to provide some essential aspects of biocomputing. Through their adaptation properties, synapses are enhancing/depressing relevant/irrelevant signals from neurons. They also provide a rich set of non-linear operations to process the spike signals from neural cells.[10] As sensors, synapses are converting chemical signals from sensed neurotransmitters into transduced post-synaptic electric signals as ionic concentration modulation. Such ambivalence existing in biology is the natural example of a non-Von Neumann computing architecture that embeds highly complex biochemical sensing at all nodes in its network, and demonstrates reciprocally the power of the local adaptation of a sensing array that programs according to its environment.

In this paper, we show how OECTs can combine these two important features for bio-signal sensing and processing. The corner stone of OECTs behavior is the transconductance, which couples ionic signals to electronic ones.[11] Transconductance can be well described by the coupling between: i) volumetric ionic capacitance allowing for a very large effective surface of interaction between the analyte and the polymer; and ii) efficient electronic transport along the π-conjugated organic chains. Several works have demonstrated routes for optimizing transconductance through either volumetric capacitance or electronic mobility tuning.[12,13] Notably, side-chain engineering on the conductive backbone of the polymer have been recently proposed as a promising chemical engineering route.[14] Here, we show how electropolymerization can be used to adapt post-fabrication of these two intrinsic parameters of OECTs (i.e., volumetric capacitance and electronic mobility) and how this technique

M. Ghazal, M. Daher Mansour, C. Scholaert, T. Dargent, Y. Coffinier, S. Pecqueur, F. Alibart
Institut d'Électronique
Microélectronique et Nanotechnologies (IEMN) – CNRS UMR 8520 – Université de Lille
boulevard Poincarré, Villeneuve d'Ascq 59652, France
E-mail: sebastien.pecqueur@univ-lille.fr; fabien.alibart@univ-lille.fr
F. Alibart
Laboratoire Nanotechnologies Nanosystèmes (LN2) – CNRS UMI-3463 – 3IT
Sherbrooke J1K 0A5, Canada

The ORCID identification number(s) for the author(s) of this article can be found under https://doi.org/10.1002/aelm.202100891.

DOI: 10.1002/aelm.202100891

results in bio-inspired adaptive sensing. We combine standard spin-coating deposition technique with post-fabrication potentiostatic electropolymerization (EP) to show how OMIECs properties can be adjusted finely. Organization of the poly(3,4-ethyle nedioxythiophene):polystyrene sulfonate (PEDOT:PSS) domains are revealed by scanning electron microscopy (SEM) and atomic force microscopy (AFM) for different EP conditions. Raman spectroscopy is used to highlight π-conjugated domains organization and redox state of the PEDOT under different deposition conditions. We combine DC electrical measurements with electrochemical impedance spectroscopy to extract volumetric capacitance and electronic mobility. These material aspects are then employed to show how transconductance of OECTs from a multi-sensor array can be adapted on-demand to an optimal transconductance value, which mimics the long-term potentiation process in biological synapses. We further demonstrate how tuning OECTs intrinsic properties can result in tunable frequency filters, which provides a unique opportunity for processing spike-based signals equivalently to short-term plasticity effects as a memory mechanism enabled in biological synapses.

2. Results and Discussion

OECTs' electrodes were realized following a conventional route involving Au source (S) and drain (D) electrodes metal patterning through optical lithography and lift-off. A two layers parylene C was subsequently used to define a 30 µm diameter opening on top of the S and D contacts. The resulting W/L for OECTs was 30/12. The first layer was used for contact line insulation while the second one acts as a sacrificial layer. PEDOT:PSS (Clevios PH1000) was first spin-coated before sacrificial layer removal resulting in a 200 nm thick spin-coated PEDOT:PSS in between S and D contacts (**Figure 1**). This standard process for OECTs fabrication results in well-established transconductance performances $Gm \propto \mu \times C^*$. Hole mobility ($\mu$) is the effective mobility of electronic carriers along the π-conjugated system and results from both delocalized states: i) intra-macromolecular π–σ–π electron delocalization along the thiophene backbone; or ii) hoping from π–π-stacked intermolecular thiophene rings; and iii) intermolecular hoping between two PEDOT macro-molecules that are adjacent to a same PSS macromolecular chain.[15] Intermolecular hoping is the most limiting mechanism that largely defines the effective mobility of electronic carriers through the material. Volumetric capacitance C^* is describing the permeability of PEDOT:PSS to ions allowing positively charged ions to interact with PSS^- fixed charges in the bulk of the material.[16,17] Direct correlation between Gm and both μ and C^* justifies why transconductance is the main figure of merit describing both ionic and electronic properties of OMIECs.[18]

It turns out that improving transconductance has been realized following either volumetric capacitance or electronic

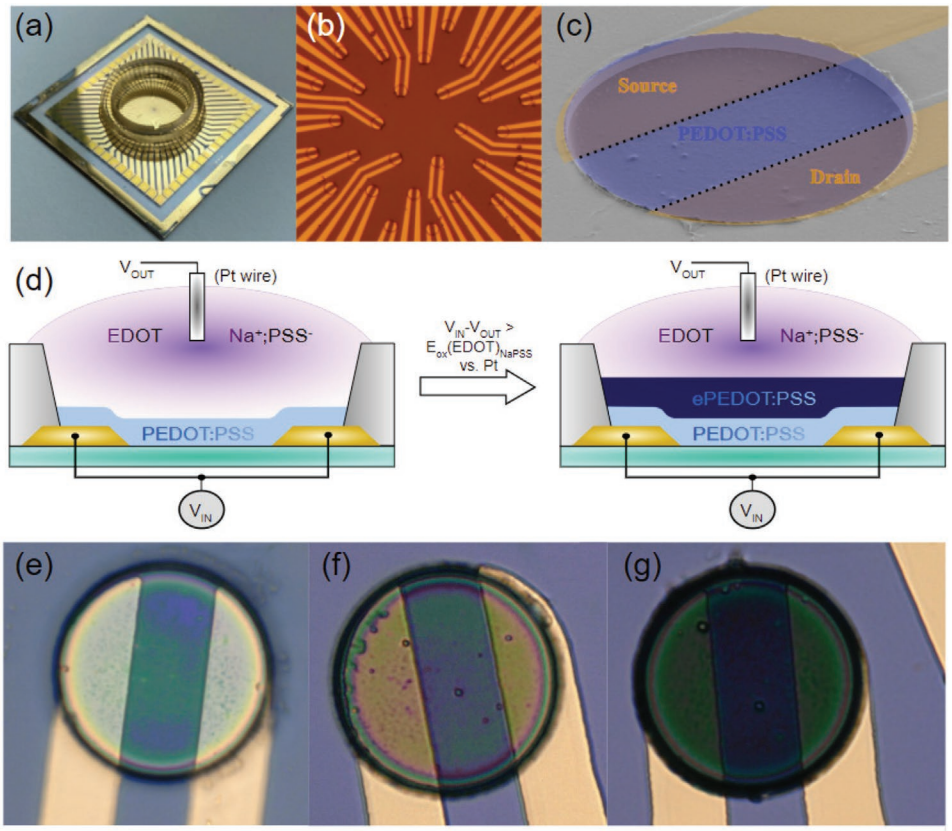

Figure 1. Electropolymerization technique for OECTs. a) OECT glass chip. b) Microscopic image of the array of 30 OECTs. c) Colorized SEM image for a PEDOT:PSS OECT. d) Schematic representation showing the experimental setup to perform potentiostatic electropolymerization of EDOT on top of spin-coated PEDOT:PSS OECT. e–g) Microscopic images (from left to right) of spin-coated PEDOT:PSS OECT, spin-coated and electropolymerized PEDOT at 0.6 V, spin-coated and electropolymerized PEDOT at 0.7 V.

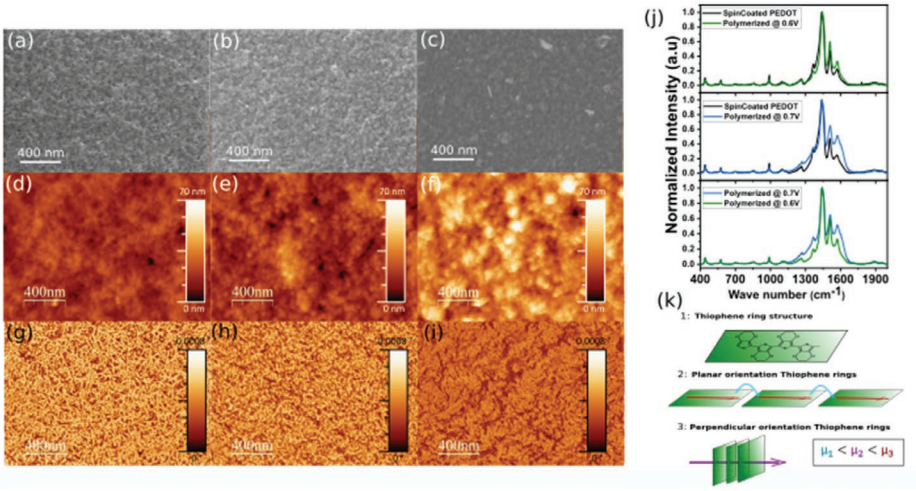

Figure 2. Impact of electropolymerization on PEDOT:PSS microstructure. a–c) SEM images of the channel material for spin-coated PEDOT:PSS, electropolymerized PEDOT at 0.6 V, and electropolymerized PEDOT at 0.7 V OECTs. d–f) AFM height images of the channel's material for spin-coated PEDOT:PSS, electropolymerized PEDOT at 0.6 V, and electropolymerized PEDOT at 0.7 V OECTs. g–i) AFM phase images of the channel material for spin-coated PEDOT:PSS, electropolymerized PEDOT at 0.6 V and electropolymerized PEDOT at 0.7 V OECTs. j) Typical Raman spectra ($\lambda_{exc} = 477$ nm) of spin coated PEDOT:PSS (in black), electropolymerized at 0.6 V (in green), and electropolymerized at 0.7 V (in blue). k) Schematic representation of the PEDOT thiophene ring structure and its planar and perpendicular orientation structure.

mobility tuning. For spin-coated PEDOT:PSS, improving volumetric capacitance has been realized by material engineering routes consisting in addition of hydrophilic chains and molecules[19,20] to the spin-coated solution that results in larger volumetric capacitance values of up to 40 F cm^{-3}. A more straightforward solution is to increase the total thickness of PEDOT:PSS in order to increase the total capacitance of the OECT.[21] This technique has resulted in record transconductance of ≈4000 µS, surpassing 2D materials mobility such as graphene.[1] Nevertheless, as a soft fabrication process, spin-coating by itself does not allow adjusting the volumetric capacitance. Successive spin-coating steps are required and lead to a poor control over the total material thickness and variability. This holds also for the control of the effective mobility (i.e., organization of the π-conjugated system in PEDOT:PSS) that is mostly defined by chemical interaction of the polymer in its solution and its kinetics for drying upon a specific process. Notably, PEDOT molecules have been reported to organize along the PSS chains resulting in a fiber-like structure.[15] Addition of heterogeneous elements in the solution have demonstrated improved mobility of spin-coated PEDOT:PSS.[22] Recently, effective mobility improvement was obtained by mechanical-stress engineering in PEDOT-PSS fibers resulting in improved organization of the π-conjugated system along the fiber with effective mobility as high as 12.9 $cm^2\ V^{-1}\cdot s^{-1}$.[23] It turns out that both capacitance and effective mobility improvement for high transconductance are only accessible via various material synthesis and engineering techniques that cannot be necessarily combined. This lack of engineering flexibility represents a strong limitation for the future development of OECTs applications.

2.1. Microstructural Analysis of Electropolymerized PEDOT:PSS

In our approach, we propose to combine spin-coating with electropolymerization in order to gain an additional level of freedom in adjusting ionic and electronic properties of OECTs. Electropolymerization (EP) has been largely investigated for PEDOT materials deposition.[24,25] Here, EP of PEDOT:PSS was realized in a potentiostatic configuration as shown in Figure 1d with S and D as working electrode (V_{IN}) and grounded Pt wire as reference electrode (V_{OUT}) dipped into the electrolyte that contained the monomer (0.01 M EDOT + 0.1 M PSSNa). EP was realized on top of a standard spin-coated layer of a PEDOT:PSS (see Experimental Section). A fiber-like structure was obtained for spin-coated PEDOT and granular structure was obtained for electropolymerized materials as shown in the scanning electron microscopy (SEM) and AFM images of **Figure 2**. Statistical analysis of these AFM images was realized to reveal the grain size, surface roughness, and thicknesses of the electropolymerized thin films. For 0.6 V EP potential, AFM images showed granular growth with a grain size of ≈5 nm whereas grains of ≈9 nm were formed for 0.7 V potential. Surface average roughness increased from ≈3, ≈4, and ≈8 nm for the spin-coated, 0.6 and 0.7 V electropolymerized PEDOT films, respectively. A clear relation between grain size and roughness can be drawn from these measurements with similar ratios of ≈1:2 for both 0.6 and 0.7 V EP potentials. Moreover, height profiles of AFM images before and after EP revealed electropolymerized thin films of (100 ± 4) and (200 ± 8) nm for 8 s of EP at 0.6 and 0.7 V, respectively. The thickness of the two thin films presented a ratio of 1:2, which might explain the increase of the roughness and the creation of a less organized surface for higher deposition rate. More interestingly, EP gave us access to various thin-film microstructures that should relate to different electrical properties of the materials.

Figure 2j shows the Raman spectra of PEDOT:PSS grown by spin-coating (black line) and by EP at 0.6 V (green line) and at 0.7 V (blue line) potentials. These spectra are typical of the ones shown in the literature for PEDOT:PSS.[26–28] The bands assignment are presented in Table S1, Supporting Information. From these measurements, we identified different orientations of polymers deposited on the surface and doping levels among the

three different deposition conditions. Concerning the doping level, the peak for the $C_\alpha = C_\beta$ symmetric vibrations shifted from 1439 cm^{-1} for the spin-coated PEDOT to 1444 cm^{-1} for both electropolymerized PEDOT. This shifts indicates a higher level of oxidation for the polymer[26,28–33] in correlation with the peaks at 1266 cm^{-1} that corresponded to the oxidized state of PEDOT.[26,28–33] In addition, these blue-shifts (i.e., to higher wavenumbers) could be associated to oxidized states with quinoid form of polymer chains, which may have a key role to play on the conductivity of the polymers.[31] Moreover, electropolymerized PEDOT at 0.6 V presented the narrowest peak at 1444 cm^{-1} which suggested a larger rate of π–σ–π conjugation and thus higher crystallinity and conductivity as shown by Zhao et al.[29,34] On the other hand, the decrease in the intensity of the peaks in the 400–1000 cm^{-1} region (dioxyethylene ring deformation) whereas an increase is observed at 1450–1650 cm^{-1} ($C_\alpha = C_\beta$ vibrations region) for both electropolymerized PEDOT relatively to spin-coated PEDOT indicated a perpendicular orientation of the thiophene rings with respect to the surface and thus an edge on the growth of PEDOT:PSS on the surface.[30,35–37] To complete the discussion on the Raman measurements, electropolymerized PEDOT at 0.6 and 0.7 V showed different intensity peaks in the 1300–1600 cm^{-1} region for the C_β–C_β stretching and the $C_\alpha = C_\beta$ asymmetric vibrations. These differences in relative intensities also indicated a different structure orientation of the polymer chains with respect to the surface, and thus different electrical properties. As illustrated in the schematic of Figure 2k, the relative orthogonality of thiophene rings organization to the substrate plane leads to a higher rate of in-plane π–π stacking which in turn increases the mobility in the thin films. In agreement, narrower peaks for PEDOT at 0.6 V indicate better crystallinity and thus better conductivity. Wu and coworkers[37] showed that a π–π stacking order in a lamella inter-chain stacking structure for an edge-on PEDOT orientation increased the conductivity of the thin-film polymer. Therefore, we can expect here a better crystallinity structure for PEDOT grown at 0.6 V with the latter ordering, which led to a better conductivity of the thin film polymer.

From a structural and organizational standpoint, the Raman and AFM results correlated. The results were in agreement with a smoother and more organized PEDOT:PSS chains for the 0.6 V EP. These different growth characteristics (thickness, organization) revealed by AFM and Raman might give us a hint on the electrical properties of the PEDOT:PSS thin films. The growth at 0.6 V potential is expected to present a better conductivity while the growth at 0.7 V is expected to present higher capacitance. These findings suggest that electrical properties can be tuned by applying different conditions of electropolymerization.

2.2. Transconductance and Impedance Evaluation

The combination of spin-coating with EP is offering an interesting option for accessing different material microstructures. Different microstructures are affecting the transconductance through a change either in capacitance or in electronic mobility. To access the ionic and electronic properties of the film, we conducted both DC electrical characterization of the OECTs and electrochemical impedance spectroscopy for various EP conditions. EP was realized sequentially on the same OECTs by steps of 2 s. Transfer characteristics and impedance spectrum were recorded between each step. In the case of OECT operation, an Ag/AgCl wire is used as a gate, while Pt was previously chosen as an electrochemically inert counter electrode for electropolymerization. While both having different roles, the choice for a same Pt wire as both a gate electrode can even be a fair compromise as an electrode acting either as an electrochemically stable counter electrode for EP and as gate for the transistor: Though former studies showed that this material choice for a gate electrode is rather limiting in depletion, the large difference in size between the OECT device and the gate compensates it, and would allow one single three-wire setup to be generic for both sensor modification and its operation. **Figure 3** presents the evolution of transfer characteristic and impedance for potentiostatic EP on top of spin-coated PEDOT:PSS at V_p = 0.6 V. Transfer characteristics provide a direct access to transconductance through $G_m = dI_{ds}/dV_g$, with I_{ds} the channel current and V_g the gate voltage. Impedance spectroscopy was modeled with an equivalent electrical circuit (Figure 3c) giving access to the total capacitance of the OECT. Combining I_D–V_G with capacitance measurement, we extracted hole mobility μ ranging from 0.3 to 1.1 $cm^2\ V^{-1}\cdot s^{-1}$ (see Supporting Information for details on μ extraction and Table S1, Supporting Information, for the absolute values). A clear increase of transconductance was observed as well as a clear increase in the capacitance (i.e., shift of the –1 slope part of the impedance modulus spectrum below 1 kHz). We conducted the same experiment for various potentiostatic conditions. Figure 3d presents the relative change of maximum transconductance as a function of the relative change of capacitance. Following the work of Rivnay et al.,[21] the dashed line in Figure 3d presents the linear relation expected in the case of a simple increase of material thickness. In this scenario, an increase of G_m is solely related to an increase of volume leading to higher capacitance. Interestingly, we observed that 0.6 V EP condition led to an evolution above this unity line while a larger potential led to an evolution below it. Since transconductance depends on capacitance, mobility, and threshold voltage,[20] these deviations from the unity line indicates that EP should also affect mobility μ and/or threshold voltage V_{th} of the OECT. We report in Figures S3a and S3b, Supporting Information, the relative change of μ and V_{th} as a function of the relative change of G_m. V_{th} showed only a weak variation (below 10%) whereas μ showed a clear dependency with G_m for the different EP conditions. A low EP potential of 0.6 V led to a higher mobility material and higher EP potentials of 0.65 and 0.7 V led to a lower mobility material with respect to spin-coated PEDOT:PSS (note that we can only access the average mobility of both spin-coated and electrodeposited PEDOT:PSS). In other words, EP provides a versatile technique that can be used to tune both electronic mobility and ionic capacitance. Note that although ionic diffusivity through PEDOT:PSS couldn't be directly evaluated on this electrical measurement protocol, EP should also modify its value due to the different morphologies observed in Figure 1. Overall, a 120% increase in the peak transconductance and 40% increase in mobility with potentiostatic EP of PEDOT:PSS OECTs is demonstrated.

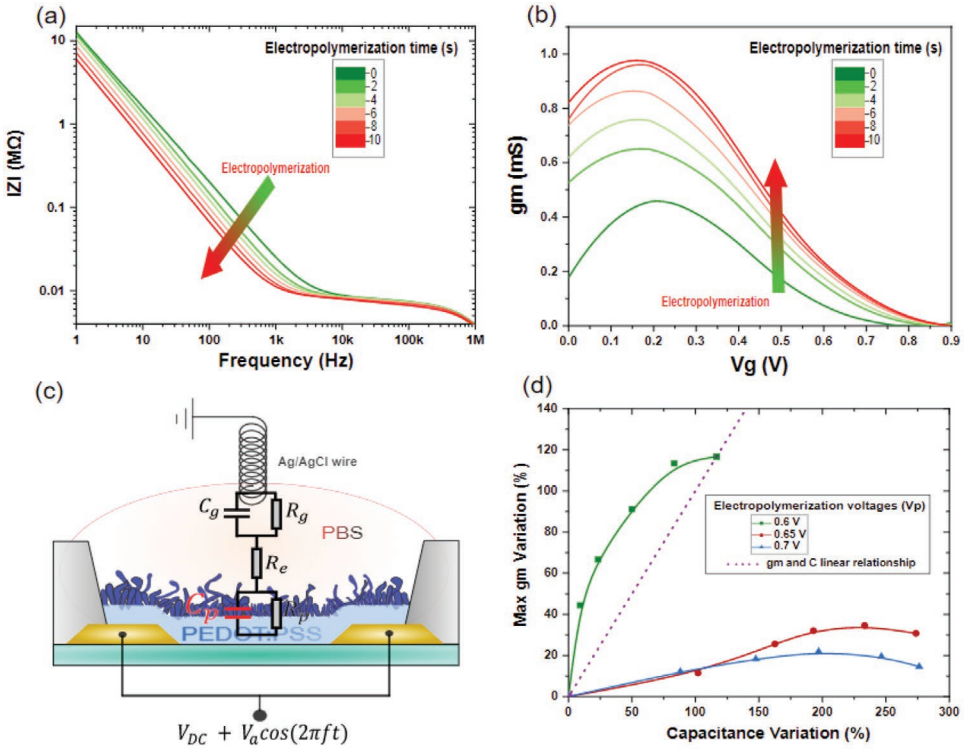

Figure 3. Impact of electropolymerization on OECTs' electrical properties. a) Bode's diagram of the impedance spectroscopy for an OECT during successive EP steps of 2 s at $V_p = 0.6$ V on top of spin-coated PEDOT:PSS. b) Effect on the transconductance for the same device as in (a). c) Equivalent electrical circuit used to extract the total capacitance C_p of the OECT. d) Correlation graph between the equivalent capacitance (from the impedance spectrogram fitting) and the device transconductance (from the OECT transfer characteristics) for different EP voltages. Each point from a line is obtained by repeating the same EP conditions for 2 s.

2.3. Capacitance and Effective Mobility Tuning for Adaptive OECTs Sensors

Versatility of electropolymerization is an attractive solution to engineer post-fabrication ionic and electronic properties in OMIECs. Having independent control over OMIECs capacitance and mobility can be used to adapt OECTs responses depending on the targeted application. In biological neural networks, synapses are experiencing long-term modification of their strength through learning to process bio-signals efficiently. This property is extensively used in an artificial neural network through supervised training of networks to implement fundamental tasks such as signal classification or feature extraction. Equivalently, tunable OECTs sensors with adaptive transconductance could be used to extract important features from the biological medium by weighting the transconductance of each sensor individually. **Figure 4**a presents the evolution of peak transconductance when successive electropolymerizations were realized to reach a 1 mS transconductance value. In our experiment, the transconductance was recorded after every

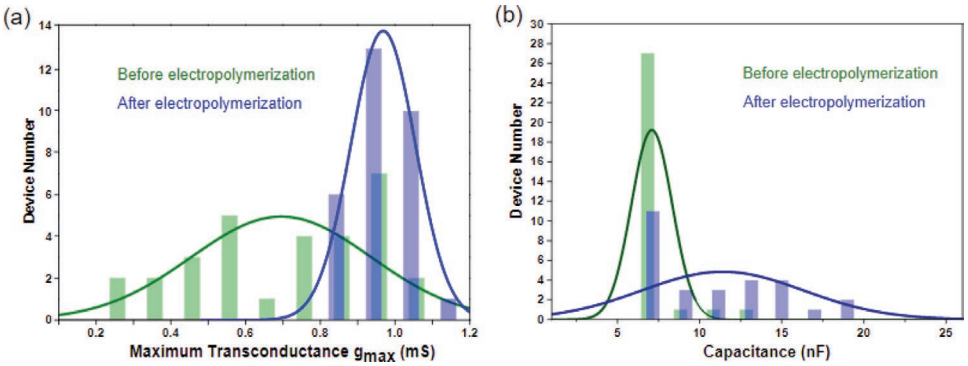

Figure 4. Adaptive OECT implementation with EP. a) Green: distribution of the maximum transconductance (mS) for an array of 30 OECTs. An adaptation procedure with target of 1 mS is used to gradually change the transconductance of each OECT sequentially. (blue) Final transconductance reach after device adaptation. b) Distribution of the capacitance before (green) and after (blue) OECT adaptation. Lines are the Gaussian fitting of the histograms.

2 s of EP. When the transconductance of more than 1 mS was reached or the EP time was larger than 10 s, the transconductance tuning was stopped. In addition to a mean transconductance value of 0.98 mS (i.e., 2% deviation from the targeted value) a large decrease of standard deviation in transconductance from 0.24 to 0.086 mS was obtained for a batch of 30 devices belonging to the same array. Figure 4b shows the evolution of the capacitance for the same experiment. The low initial variability in capacitance associated to the large initial variability in the transconductance of spin-coated PEDOT:PSS points to variability in mobility rather than variability in capacitance as the initial source of variability in transconductance. The increase in capacitance variability after EP suggests that variability in transconductance was reduced by adjusting capacitance rather than mobility. It is to note that transconductance tuning could be optimized further by using an automated setup that could allow for fine-tuning over time by combining EP and transconductance measurements in the same environment. In our case, the setup was limited by the manual operation. Also, this demonstration implemented only long-term potentiation effects (i.e., increase of the transconductance). As suggested by the decay of transconductance for a long EP time in Figure 3d, long-term depressions (LTD) should also be available. The origin of LTD could be explained by either: i) a degradation of mobility of the previously deposited material by decreasing thiophene rings organization when more material was added; or ii) ions diffusivity limitation when too thick materials are deposited. Further investigations are required to conclude on this aspect. We also note that both LTP and LTD are irreversible mechanisms. By analogy with biological cells, which show different forms of plasticity, combining these structural modifications with long-term doping/de-doping of the PEDOT:PSS could offer more flexibility for OECT programming in the context of adaptive and plastic sensors.

A second bio-inspired feature available with adaptive OECTs is to implement short term plasticity (STP). Here we capitalized on the bottom-up tuning of OECTs capacitance to show how an additional degree of freedom can be obtained with EP. **Figures 5**a and b compare the response to a train of 100 µs pulses at 1 and 8 kHz before and after EP, respectively. The STP effect results from the balance in between the ions charging during the 200 mV pulse and discharging during the 0 V inter-pulse interval. After EP at 0.7 V, the capacitance of the OECT was increased from 10 to 19 nF, thus increasing the time constant of the equivalent resistor–capacitor circuit. Before EP, OECTs response presented higher modulation than after EP at low frequency. Note that in this low frequency regime, charge and discharge were completely balanced. At high frequency, both devices reached an equivalent saturation regime corresponding to the maximal accumulation of positive ions. In this later case, charging was not balanced by discharging due to the short inter-pulse interval and the current reached the saturation level. Comparison between the two responses demonstrates the possibility to tune the high-pass filtering property of the OECT with EP. For instance, OECT after EP can discriminate the low frequency signals from the high frequency one whereas it cannot before EP. It was recently proposed that STP effects in neural networks can be modeled as a combination of various frequency filters.[38] Here, the adaptive property of OECTs with in-situ EP represents an attractive feature for neuromorphic synapses engineering that could allow us to reproduce complex STP mechanisms.

3. Conclusion

We report in this paper on the utilization of EP as an in-situ technique for tuning the iono-electronic properties of OECTs. OMIEC optimization has been largely proposed with either volumetric capacitance or effective mobility tuning. We showed here that EP provided a unique technique that allowed for the controlling of both properties simultaneously. This solution is opening new perspectives for the engineering of OECTs where transconductance and impedance can be finely adjusted. More fundamentally, this work is showing how ionic and electronic properties are governing the OECTs responses (see Figure S3, Supporting Information), which contributes to a better understanding of mixed ionic electronic processes in OMIECs.

Along this line, an important bottleneck of OECTs development as bio-sensors is associated with the large variability

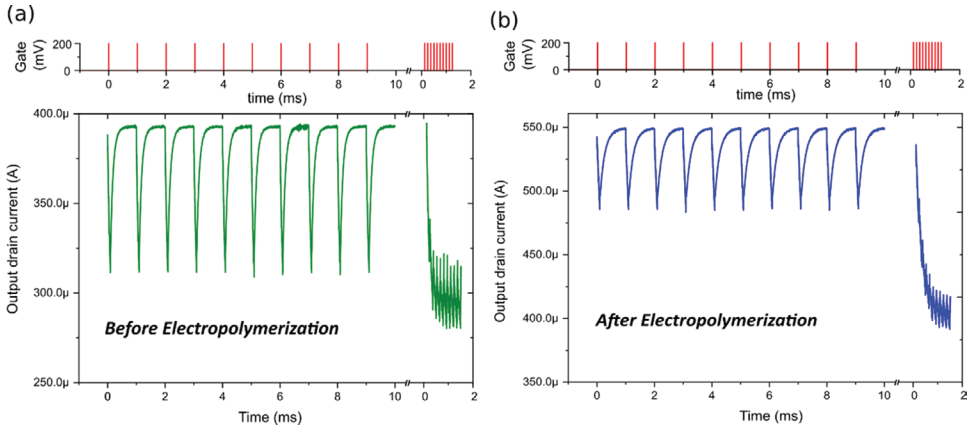

Figure 5. Capacitance tuning for adaptive OECTs sensors. Current output response to a train of 100 µs and 200 mV pulses on the gate electrode at 1 and 8 KHz of an OECT before (a) and after (b) capacitive tuning by EP. EP allows tuning the frequency response of the OECT with a clear discrimination of the low/high frequency signal after EP and a low discrimination before EP.

of soft technologies when circuits and systems need to be designed. Spin-coating as well as inkjet printing, which are the most popular OMIECs fabrication routes, are room-temperature and ambient atmosphere deposition conditions that are prone to high amount of defects in the OMIECs. EP can offer an interesting alternative to adjust the iono-electronic properties of the material post-fabrication to match a tolerable range of variability in these properties. Notably, we showed that standard deviation in transconductance can be reduced by 60%.

This approach is also offering a new strategy for the development of adaptive sensors that can adapt to their sensing environment. For instance, electrophysiological recording could benefit from sensor arrays that could be adapted to the specific organization of the biological neural network. Equivalently to learning, adaptive protocols could be designed to adjust the OECTs response to match biological neural network organization. It has to be noted that EDOT molecules are non-cytotoxic[39,40]—at least in the range of concentration reported in this study—and PSS:Na is non acidic. Future work could consider in-situ EP with living cells in the medium. In addition, since electro-active cells/electrode coupling is based on capacitive effect, OECTs fine-tuning can be used to optimize cells/OECTs coupling or to adjust the filtering of complex bio-signals. Finally, EP can also open new perspectives for the development of non-standard OECTs structures that are not bounded to standard top-down design technics. Along this line, electropolymerized dendritic OECTs are emerging as a new direction for bio-inspired computing deployment.[41]

4. Experimental Section

Materials and Instrumentation: Electropolymerization was done by potentiostatic configuration in an aqueous electrolyte containing 0.1 M of poly(sodium-4-styrene sulfonate) (NaPSS) and 0.01 M of 3,4-ethylenedioxythiophene (EDOT). All chemicals were purchased from Sigma Aldrich. Source and drain as working electrode (V_{IN}) and grounded Pt wire as counter electrode (V_{OUT}) dipped into the electrolyte.

Raman: A 473 nm excitation laser (≈1 mW) focused with a 100× objective was used for confocal Raman spectroscopy measurements in air at room temperature. Raman data were treated with Labspec5 software provided by Bruker.

AFM: ICON, Bruker AFM, tapping, and phase mode images taken in air atmosphere at room temperature ≈293 K. The authors used Si cantilevers with a free oscillating frequency $f_0 \approx 320$ kHz and a spring constant $k \approx 42$ N m^{-1}. AFM images were treated with Gwyddion.[42]

Optical Microscopic Images: Optical microscopic images were done with a Keyence numerical microscope.

Electrical Characterization: The transistors were characterized using a PBS solution as the electrolyte. An Ag/AgCl wire was immersed in the electrolyte and used as the gate electrode. The same type of wire was used as a gate electrode during electrochemical impedance spectroscopy (see below). Agilent B1500A semiconductor device analyzer was used to bias the transistor and record the drain current.

Electrochemical Impedance Spectroscopy (EIS): EIS was performed with a Solartron Analytical (Ametek) impedance analyzer from 1 MHz to 1 Hz. All impedance measurements were done in the same electrical ($V_{DC} = 100$ mV and $V_a = 20$ mV) and electrochemical conditions (PBS as electrolyte). Source and drain as working electrode (V_{IN}) and grounded Ag/AgCl wire as reference electrode (V_{OUT}) dipped into the electrolyte.

Circuit Impedance Modeling: Circuit impedance modeling was performed using an open-source EIS Spectrum Analyzer software.[43] The RC parameter fitting was manually adjusted by simultaneous comparison of the Nyquist plots, Bode's modulus, and Bode's phase plots.

Supporting Information

Supporting Information is available from the Wiley Online Library or from the author.

Acknowledgements

The authors thank the RENATECH network and the engineers from IEMN for their support. This work is founded by ERC-CoG IONOS project #773 228.

Conflict of Interest

The authors declare no conflict of interest.

Data Availability Statement

Research data are not shared.

Keywords

adaptive sensors, biosensors, electropolymerization, organic electrochemical transistors, PEDOT:PSS

Received: August 21, 2021
Revised: October 13, 2021
Published online: November 10, 2021

[1] D. Khodagholy, T. Doublet, P. Quilichini, M. Gurfinkel, P. Leleux, A. Ghestem, E. Ismailova, T. Hervé, S. Sanaur, C. Bernard, G. G. Malliaras, *Nat. Commun.* **2013**, *4*, 1575.
[2] J. Rivnay, S. Inal, A. Salleo, R. M. Owens, M. Berggren, G. G. Malliaras, *Nat. Rev. Mater.* **2018**, *3*, 17086.
[3] P. Gkoupidenis, N. Schaefer, B. Garlan, G. G. Malliaras, *Adv. Mater.* **2015**, *27*, 7176.
[4] D. A. Bernards, G. G. Malliaras, *Adv. Funct. Mater.* **2007**, *17*, 3538.
[5] C. Yao, Q. Li, J. Guo, F. Yan, I.-M. Hsing, *Adv. Healthcare Mater.* **2015**, *4*, 528.
[6] X. Ji, B. D. Paulsen, G. K. K. Chik, R. Wu, Y. Yin, P. K. L. Chan, J. Rivnay, *Nat. Commun.* **2021**, *12*, 2480.
[7] J. Y. Gerasimov, R. Gabrielsson, R. Forchheimer, E. Stavrinidou, D. T. Simon, M. Berggren, S. Fabiano, *Adv. Sci.* **2019**, *6*, 1801339.
[8] S. Pecqueur, M. M. Talamo, D. Guérin, P. Blanchard, J. Roncali, D. Vuillaume, F. Alibart, *Adv. Electron. Mater.* **2018**, *4*, 1800166.
[9] P. Gkoupidenis, N. Schaefer, X. Strakosas, J. A. Fairfield, G. G. Malliaras, *Appl. Phys. Lett.* **2015**, *107*, 263302.
[10] F. Zenke, E. J. Agnes, W. Gerstner, *Nat. Commun.* **2015**, *6*, 6922.
[11] D. Khodagholy, J. Rivnay, M. Sessolo, M. Gurfinkel, P. Leleux, L. H. Jimison, E. Stavrinidou, T. Herve, S. Sanaur, R. M. Owens, G. G. Malliaras, *Nat. Commun.* **2013**, *4*, 2133.
[12] P. R. Paudel, V. Kaphle, D. Dahal, R. K. Radha Krishnan, B. Lüssem, *Adv. Funct. Mater.* **2021**, *31*, 2004939.
[13] A. F. Paterson, A. Savva, S. Wustoni, L. Tsetseris, B. D. Paulsen, H. Faber, A. H. Emwas, X. Chen, G. Nikiforidis, T. C. Hidalgo, M. Moser, I. P. Maria, J. Rivnay, I. McCulloch, T. D. Anthopoulos, S. Inal, *Nat. Commun.* **2020**, *11*, 3004.
[14] A. L. Jones, M. De Keersmaecker, L. R. Savagian, B. T. DiTullio, I. Pelse, J. R. Reynolds, *Adv. Funct. Mater.* **2021**, *31*, 2102688.
[15] M. N. Gueye, A. Carella, J. Faure-Vincent, R. Demadrille, J.-P. Simonato, *Prog. Mater. Sci.* **2020**, *108*, 100616.

[16] C. M. Proctor, J. Rivnay, G. G. Malliaras, *J. Polym. Sci., Part B: Polym. Phys.* **2016**, *54*, 1433.
[17] A. V. Volkov, K. Wijeratne, E. Mitraka, U. Ail, D. Zhao, K. Tybrandt, J. W. Andreasen, M. Berggren, X. Crispin, I. V. Zozoulenko, *Adv. Funct. Mater.* **2017**, *27*, 1700329.
[18] S. Inal, G. G. Malliaras, J. Rivnay, *Nat. Commun.* **2017**, *8*, 1767.
[19] A. Giovannitti, D.-T. Sbircea, S. Inal, C. B. Nielsen, E. Bandiello, D. A. Hanifi, M. Sessolo, G. G. Malliaras, I. McCulloch, J. Rivnay, *Proc. Natl. Acad. Sci. USA* **2016**, *113*, 12017.
[20] P. Schmode, A. Savva, R. Kahl, D. Ohayon, F. Meichsner, O. Dolynchuk, T. Thurn-Albrecht, S. Inal, M. Thelakkat, *ACS Appl. Mater. Interfaces* **2020**, *12*, 13029.
[21] J. Rivnay, P. Leleux, M. Ferro, M. Sessolo, A. Williamson, D. A. Koutsouras, D. Khodagholy, M. Ramuz, X. Strakosas, R. M. Owens, C. Benar, J.-M. Badier, C. Bernard, G. G. Malliaras, *Sci. Adv.* **2015**, *1*, e1400251.
[22] Y. H. Kim, C. Sachse, M. L. Machala, C. May, L. Müller-Meskamp, K. Leo, *Adv. Funct. Mater.* **2011**, *21*, 1076.
[23] Y. Kim, H. Noh, B. D. Paulsen, J. Kim, I.-Y. Jo, H. Ahn, J. Rivnay, M.-H. Yoon, *Adv. Mater.* **2021**, *33*, 2007550.
[24] B. Ji, M. Wang, *J. Micromech. Microeng.* **2020**, *30*, 104001.
[25] B. Ji, M. Wang, C. Ge, Z. Xie, Z. Guo, W. Hong, X. Gu, L. Wang, Z. Yi, C. Jiang, B. Yang, X. Wang, X. Li, C. Li, J. Liu, *Biosens. Bioelectron.* **2019**, *135*, 181.
[26] S. Garreau, J. L. Duvail, G. Louarn, *Synth. Met.* **2001**, *125*, 325.
[27] S. Garreau, G. Louarn, J. P. Buisson, G. Froyer, S. Lefrant, *Macromolecules* **1999**, *32*, 6807.
[28] S. Sakamoto, M. Okumura, Z. Zhao, Y. Furukawa, *Chem. Phys. Lett.* **2005**, *412*, 395.
[29] Q. Zhao, R. Jamal, L. Zhang, M. Wang, T. Abdiryim, *Nanoscale Res. Lett.* **2014**, *9*, 557.
[30] E. Tamburri, S. Orlanducci, F. Toschi, M. L. Terranova, D. Passeri, *Synth. Met.* **2009**, *159*, 406.
[31] W. W. Chiu, J. Travaš-Sejdić, R. P. Cooney, G. A. Bowmaker, *Synth. Met.* **2005**, *155*, 80.
[32] P. V. Almeida, C. M. S. Izumi, H. F. D. Santos, A. C. Sant'Ana, *Química Nova* **2019**, *42*, 1073.
[33] W. W. Chiu, J. Travaš-Sejdić, R. P. Cooney, G. A. Bowmaker, *J. Raman Spectrosc.* **2006**, *37*, 1354.
[34] J. L. Duvail, P. Rétho, S. Garreau, G. Louarn, C. Godon, S. Demoustier-Champagne, *Synth. Met.* **2002**, *131*, 123.
[35] B. R. Moraes, N. S. Campos, C. M. S. Izumi, *Vib. Spectrosc.* **2018**, *96*, 137.
[36] N. Sakmeche, S. Aeiyach, J.-J. Aaron, M. Jouini, J. C. Lacroix, P.-C. Lacaze, *Langmuir* **1999**, *15*, 2566.
[37] D. Wu, J. Zhang, W. Dong, H. Chen, X. Huang, B. Sun, L. Chen, *Synth. Met.* **2013**, *176*, 86.
[38] E. M. Izhikevich, N. S. Desai, E. C. Walcott, F. C. Hoppensteadt, *Trends Neurosci.* **2003**, *26*, 161.
[39] L. Ouyang, C. L. Shaw, C.-C. Kuo, A. L. Griffin, D. C. Martin, *J. Neural Eng.* **2014**, *11*, 026005.
[40] Y. Chen, W. Pei, S. Chen, X. Wu, S. Zhao, H. Wang, H. Chen, *Sens. Actuators, B* **2013**, *188*, 747.
[41] M. Cucchi, C. Gruener, L. Petrauskas, P. Steiner, H. Tseng, A. Fischer, B. Penkovsky, C. Matthus, P. Birkholz, H. Kleemann, K. Leo, *Sci. Adv.* **2021**, *7*, 34.
[42] D. Nečas, P. Klapetek, *Open Phys.* **2011**, *10*, 181.
[43] A. S. Bondarenko, G. A. Ragoisha, *J. Solid State Electrochem.* **2005**, *9*, 845.